C.L. Bottasso, A. Croce, F. Gualdoni, P. Montinari
*Load Mitigation for Wind Turbines by a Passive Aeroelastic Device*
Journal of Wind Engineering and Industrial Aerodynamics, Vol. 148, 2016, p. 57-69
doi:10.1016/j.jweia.2015.11.001

# Load mitigation for wind turbines by a passive aeroelastic device

Carlo L. Bottasso[a,b,*], Alessandro Croce[b], Federico Gualdoni[b], Pierluigi Montinari[b]

[a] *Wind Energy Institute, Technische Universität München, D-85748 Garching b. München, Germany*
[b] *Department of Aerospace Science and Technology, Politecnico di Milano, 20156 Milano, Italy*

**Abstract**

This paper conducts a preliminary investigation of a novel passive concept for the mitigation of loads on wind turbines. The device, which can be implemented as a flap or a pitching blade tip, moves passively in response to blade vibrations, opposing them, thereby yielding an attenuation of loads. In comparison to active load mitigation devices, such as active flaps, this solution has the advantage of not requiring sensors nor actuators, resulting in a particularly simple implementation, with potential benefits in manufacturing and maintenance costs, as well as in reliability and availability.

The paper first describes the novel passive device, here implemented by means of a flap, highlighting its main characteristics. A proof of concept of the new idea is then given by a simulation study conducted with the combination of a sectional model of the flap and an aeroservoelastic multibody model of the rest of the machine. Results, obtained for a 10 MW wind turbine, indicate the ability of the passive flap in attenuating blade vibrations in a significant frequency range, which in turn yield a reduced fatigue damage to the structure without noticeable effects in terms of power production and ultimate loads.

*Keywords:*

Wind turbine, Load mitigation, Passive flap, Aeroelasticity, Wind turbine control

**Notation**

| | |
|---|---|
| $a$ | Non-dimensional distance between elastic axis and section mid chord |
| $b$ | Section semi-chord |
| $c$ | Section chord |
| $c_h, c_\theta, c_\delta$ | Plunge, torsion and flap dampings |
| $e$ | Distance between flap hinge and mid chord |
| $h$ | Plunge motion |
| $k_h, k_\theta, k_\delta$ | Plunge, torsion and flap stiffnesses |
| $l$ | Distance between flap hinge and airfoil trailing edge |

*Corresponding author, Tel.: +49 (0)89 289 16680.
*Email address:* carlo.bottasso@tum.de (Carlo L. Bottasso)

| | |
|---|---|
| $m$ | Mass |
| $q$ | Dynamic pressure |
| $s$ | Complex number frequency |
| $s'$ | Reduced frequency |
| $t$ | Time |
| $C_H$ | Hinge moment coefficient |
| $C_L$ | Lift coefficient |
| $C_M$ | Moment coefficient |
| $J$ | Inertia |
| $U$ | Flow speed |
| $V$ | Wind speed |
| $\boldsymbol{u}$ | Input vector |
| $\boldsymbol{x}$ | State vector |
| $\boldsymbol{A}$ | Aerodynamic matrix |
| $\boldsymbol{C}$ | Damping matrix |
| $\boldsymbol{K}$ | Stiffness matrix |
| $\boldsymbol{M}$ | Mass matrix |
| $\mathscr{C}$ | Theodorsen function |
| $\alpha$ | Angle of attack |
| $\beta$ | Blade pitch |
| $\delta$ | Flap deflection |
| $\rho$ | Air density |
| $\theta$ | Torsional rotation |
| $\Omega$ | Rotor angular speed |
| $(\cdot)^C$ | Circulatory term |
| $(\cdot)^G$ | Turbulent fluctuation term |
| $(\cdot)^{NC}$ | Non-circulatory term |
| $(\cdot)_r$ | Rated quantity |
| $(\cdot)_S$ | Structural term |
| $(\cdot)_{QS}$ | Quasi-stationary term |
| $(\cdot)_{/*}$ | Partial derivative, $\partial \cdot / \partial *$ |
| $\dot{(\cdot)}$ | Derivative wrt time, $\mathrm{d} \cdot / \mathrm{d}t$ |
| AEP | Annual energy production |
| AoA | Angle of attack |

| | |
|---|---|
| BEM | Blade element momentum |
| BTC | Bend twist coupling |
| CoE | Cost of energy |
| DEL | Damage equivalent load |
| DLC | Dynamic load case |
| ETM | Extreme turbulence model |
| FEM | Finite element method |
| HAWT | Horizontal axis wind turbine |
| LQR | Linear quadratic regulator |
| LTI | Linear time invariant |
| NTM | Normal turbulence model |
| RWT | Reference wind turbine |

## 1. Introduction and motivation

In recent years, a desire to increase wind turbine dimensions while escaping the cubic law of growth has spurred an ever increasing attention to techniques for load alleviation. In fact, the mitigation of both ultimate and fatigue loads may translate into lighter weight or reduced use of high performance materials, or it can even be exploited by designing larger rotors that capture more energy.

In principle, load alleviation can be achieved by active or by passive techniques. Active solutions include full span blade pitch, as well as active flaps, tabs or other flow control devices. While full span active pitch is a standard solution on virtually all modern horizontal axis wind turbines, it has a limited bandwidth both in space and time as it can only react to relatively large and slow turbulent eddies in the flow. To address these limits, active local devices may offer a substantial bandwidth increase with a faster and more localized response, which however comes at the cost of additional complexity. In fact, the presence of sensors, actuators and moving parts may significantly increase manufacturing, maintenance and repair costs, and may reduce availability. It is not yet clear to what extent these contrasting effects may actually provide a final effective benefit in terms of the Cost of Energy (CoE).

On the other hand, passive load alleviation techniques typically do not necessitate of sensors or actuators, resulting in simpler implementations that may have a reduced or even negligible impact on maintenance, repair and availability. Bend-twist coupling (BTC), which may be obtained by the use of anisotropic materials and/or blade sweep, is very effective from this point of view because there are not only no sensors and actuators, but also no moving parts. However, similarly to blade pitch, BTC involves a full span response that may only react to large and slow wind fluctuations.

As for the active case, even for the passive solution a higher bandwidth can be achieved by using local devices, as first studied in the fixed and rotary wing literature. One of the first examples of gust-alleviating passive flaps

can be found in Doney and Shufflebarger (1940). That study developed an experimental setup for investigating in a wind tunnel the effects of a long-period dynamically overbalanced flap on a fixed wing aircraft. Results indicated a reduction of accelerations due to gusts, which was however accompanied by a decrease in stability of the vehicle. For rotorcraft applications, an analytical investigation of various aeroelastic devices appended to rotor blades is reported by Bielawa (1984). Among different solutions, a passive trailing edge tab concept is considered in that work using a simplified analysis. That study highlighted the crucial importance of tuning, since the tab motion must be phased in a correct manner to reduce the blade harmonic loads that induce vibrations to the mast. Although results appeared to be promising, the device appeared to be counter-productive when examined more carefully with its overall effects. Another passive rotorcraft appended device, similar to the passive flap, is the free tip rotor, as reported by Stroub (1982). In this solution, the blade is modified in its outer part to embed a free pitching tip. This device smooths the airload distribution in the blade tip region as the blade travels azimuthally over the rotor disk. Passive control strategies are applied to modulate the torsional moment applied to the free-tip. Different solutions are shown by Young (1986), which also reports sketches of the various design concepts.

Although these studies did show the general ability of passive devices of decreasing loads, these advantages are typically offset by an increase of weight, to the point that passive solutions do not seem nowadays to be commonly employed in aeronautical applications. The situation appears to be somewhat different in the wind energy field. In fact here, although weight is certainly a concern, the key design figure of merit is the CoE, a quantity that captures the effects of all aspects of the design of a machine over its entire lifetime. For a given load reduction achievable by two devices, the one that might actually bring a benefit to the CoE is the one that is less expensive to manufacture but also, and often more importantly, that is less costly to maintain and that ensures a greater availability. These aspects might be even more important for offshore operations, or in general in remote and difficult to reach locations, where simplicity and robustness might be particularly desirable features.

A first application in wind energy of a passive distributed system for load alleviation is analyzed by Lambie et al. (2011). A passive camber control concept is investigated, considering a 2D aeroelastic typical section. A variation of airfoil camber is obtained by exploiting the chordwise aerodynamic load distribution, which changes as a function of the angle of attack, while the original shape is restored by the use of a spring and damper. Three simplified load cases are evaluated, showing a significant decrease of load fluctuations. This device will however not only respond to undesired changes of angle of attack due to blade vibrations, but also to the deliberate changes caused by the full span pitching of the active control system that is responsible for the normal operation of the machine. In this sense, this passive device will work against the wind turbine active controller, something that casts some doubts on the actual final benefits of this particular solution. Passive load alleviation can also be achieved by structural morphing, as reported by Arrieta et al. (2012). A bi-stable specimen is designed in that work, by tailoring using an orthotropic material. When the applied load exceeds a threshold value, the structure switches from the reference state to a second statically stable one that generates less lift. This process does not require moving parts, but the main drawback is that an active

component is needed to restore the original shape (see also Arrieta et al., 2014).

The passive concept proposed in this work merges the advantages of high bandwidth distributed control with the reliability of a passive device. In a nutshell, the main idea is to use one or more flaps at suitable locations along the blade span. Such flaps are conceived so as to move in response to blade vibrations in order to oppose them. This is obtained by offsetting a mass with respect to the flap hinge, so that when the blade accelerates in one direction the flap is automatically deflected in the other, resulting in a change of camber that opposes blade motion.

Notice that the same concept could also be implemented by a freely pitching blade tip. Even in that embodiment of the idea, the working principle would remain the same, as an offset mass would drive pitching tip motions to create aerodynamic loads in opposition to blade vibrations. The remainder of this feasibility study considers the sole case of the passive flap, but the passive pitching tip remains an equally interesting possibility that will be explored in future studies.

While passive flaps and blade tips have been used in the aeronautical field, as previously mentioned, to the authors' knowledge the application of this concept to wind energy has not been described before.

As this technology should work seamlessly with other standard technologies used on board wind turbines, the passive device concept developed herein for wind energy applications satisfies by design some additional requirements. First, the presence of the device should not interfere with active full span blade pitching. In other words, the device should not move in response to changes of angle of attack due to changes in pitch, but only to changes in angle of attack due to blade deflections. This is obtained by aerodynamic balancing, i.e. by ensuring that the derivative of the device hinge moment with respect to the angle of attack is null or very small. Second, integration of the proposed device with a blade should not require a radical redesign of the blade and a drastic change in its manufacturing technology. With respect to the implementation by a flap of the passive device concept, this is obtained by using a standard trailing edge hinged flap, and by sizing the offset mass in such a way that its motion remains confined within the internal void that exists between the suction/pressure sides of the airfoil.

The paper is organized according to the following plan. At first, a simplified mathematical model is developed, to verify the feasibility of the proposed concept and to enable the assessment of its main key characteristics. The model considered here is of a hybrid nature: a complete 3D aeroservoelastic model of the wind turbine is used for generating realistic operating conditions at a blade section, which are then in turn fed to a 2D typical section model of the airfoil equipped with the passive flap. Next, the model is used for the tuning of the main design parameters of the new device. Simulations are then conducted with the goal of assessing the stability of the system, its load reduction capabilities in turbulent wind conditions and under deterministic gusts, as well as its effects on power output. Finally, conclusions are drawn and a plan for further developments is sketched.

## 2. Models and methods

Figure 1 shows a wind turbine equipped with one passive flap per blade located at 75% span, which is the configuration considered in this study, although in principle other more complex arrangements are clearly possible. Each flap moves freely and passively in response to blade vibrations, in turn modifying the aerodynamic force distribution around the blade span interval that it occupies, as shown in the picture.

Figure 1: Wind turbine equipped with passive flaps.

The loosely-coupled hybrid model depicted in Fig. 2 is used in this work. The model comprises a 3D aeroservoelastic model of the machine, implemented in the flexible multibody code `Cp-Lambda` (Code for Performance, Loads, Aeroelasticity by Multi-Body Dynamic Analysis) (Bottasso and Croce, 2006–2015), and a 2D typical section model. As shown in the picture, the 3D model is used for generating realistic inflow conditions at the blade section. When necessary, a loose coupling strategy is used to connect the 2D and 3D models, by transferring the sectional aerodynamic force perturbations generated by the use of the passive flap back onto the 3D model. A monolithic model of the machine equipped with the flaps will be developed in a continuation of this study. However, for the preliminary investigation of the passive flap concept that is the object of the present work, the simpler hybrid model was deemed sufficient. In addition, as shown later on, the 2D typical section model provides a wealth of information that is very useful for an initial understanding of the behavior of the system and its sizing.

### *2.1. 3D aeroservoelastic model*

The 3D aeroservoelastic model is based on a multibody formulation for flexible systems with general topologies. The modeling environment features a library of elements, which include rigid bodies, nonlinear flexible elements,

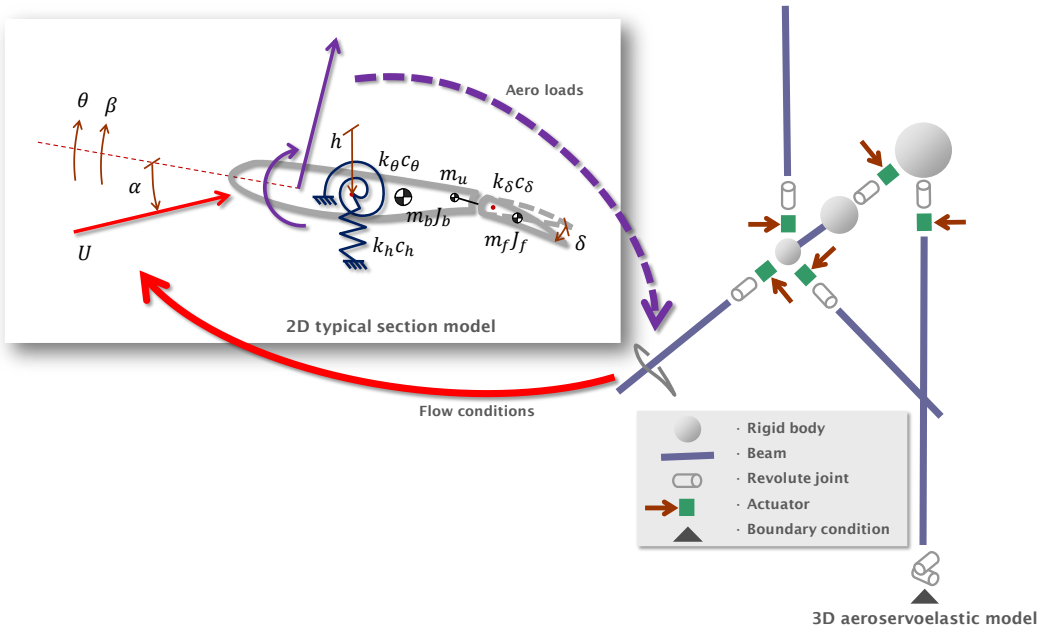


Figure 2: Hybrid simulation model. At right, 3D aeroservoelastic multibody model of the wind turbine. At left, 2D typical section model with passive flap.

joints, actuators and aerodynamic models. Sensor and control elements enable the implementation of generic control laws. The index-3 formulation is expressed in terms of Cartesian coordinates, while constraints are enforced by scaled Lagrange multipliers (Bauchau et al., 2009).

Rotor blades and tower are described by nonlinear geometrically exact shear and torsion deformable beam models, including off-diagonal stiffness couplings. Flexible components are discretized in space by the finite element method, leading to a system of differential algebraic equations in the time domain. Time integration is performed by a non-linearly unconditionally stable scheme that includes high frequency dissipation by energy decay (Bauchau et al., 2003).

The blade aerodynamic characteristics are defined by lifting lines, which include the spanwise chord and twist distributions as well as sectional aerodynamic coefficients, given in tabular form and parameterized in terms of the Reynolds number. The effects of the wake are modelled by a classical blade-element momentum (BEM) model based on annular stream tube theory with wake swirl and unsteady correction (Hansen, 2008). The aerodynamic description is completed by root and blade tip losses, unsteady aerodynamic corrections, dynamic stall, 3D blade root delayed stall and rotor-tower interference models. The wind field includes deterministic gusts and turbulent time histories, which may be obtained by the open-source software `TurbSim` (Kelley and Jonkman, 2015).

The machine is governed over its entire operating range by controllers interfaced with the wind turbine model by external dynamic libraries. A supervisory unit manages the machine behavior by switching among different operating states and handling emergencies. The model is completed by a collective-pitch/torque controller, based here on a speed-

scheduled linear quadratic regulator (LQR) (Bottasso et al., 2013), capable of controlling the machine over its entire operating envelope.

### *2.2. 2D typical section model*

The 2D sectional model is directly obtained from the modal condensation of the multibody model (for example, see Bisplinghoff and Ashley, 1962; Lambie et al., 2011), with the addition of a movable flap. This reduced order dynamical model has three degrees of freedom: the plunge motion $h$, which models the flapwise deflection of the blade, the torsional rotation $\theta$ about the elastic axis, and the flap deflection $\delta$. The plunge and twist degrees of freedom are associated with mass $m_b$, inertia $J_b$, stiffness $k_h$ and $k_\theta$, as well as damping $c_h$ and $c_\theta$, chosen so as to match the first flapwise and torsional mode frequencies and structural dampings of the rotor. Both the plunging and torsional stiffnesses depend on rotor speed, on account of centrifugal effects, i.e. $k = k_0 + k_\Omega \Omega^2$, where $k_0$ and $k_\Omega$ were tuned for each mode based on an eigenanalysis conducted with the 3D aeroelastic model.

The flap has a mass $m_f$ and an inertia $J_f$. In addition, the flap has an offset mass $m_u$, which is located forward of the flap and that moves within the void existing in that part of the blade between the suction and pressure sides of the airfoil. The offset mass is subjected to accelerations when the blade vibrates, that in turn drive the deflection of the flap to which it is connected, thereby creating aerodynamic forces that oppose the blade vibration itself. The maximum positive and negative flap deflections are limited by the thickness of the blade at the flap location, and by the position of the balancing offset mass. The flap is connected to the blade by a hinge, which features an internal rotational stiffness $k_\delta$ and damping $c_\delta$. As for plunge and torsion, even the flap stiffness can be expressed as

$$k_\delta = k_{\delta_0} + k_{\delta_\Omega} \Omega^2, \tag{1}$$

where $k_{\delta_0}$ is the spring stiffness, while $k_{\delta_\Omega}$ is due to centrifugal effects and it is negative when the flap mass lies between the elastic axis and the flap hinge, as in the present case. The hinge location is aft of the flap leading edge, in order to realize an aerodynamic balancing that reduces the sensitivity of the aerodynamic hinge moment to changes in the angle of attack.

The aerodynamic loads on the blade section are computed using classical unsteady strip theory under the hypotheses of inviscid and incompressible flow. Considering a small disturbance assumption, a closed form solution can be found in the frequency domain by the approach of Theodorsen (Theodorsen and Garrik, 1935, 1942). This classical approach is widely used to estimate the stability of the typical section. The resulting aeroelastic system writes

$$\left(\boldsymbol{M}_S s^2 + \boldsymbol{C}_S s + \boldsymbol{K}_S\right) \left\{ \begin{array}{c} h(s)/b \\ \theta(s) \\ \delta(s) \end{array} \right\} = q\boldsymbol{A}\left(s'\right) \left\{ \begin{array}{c} h(s)/b \\ \theta(s) \\ \delta(s) \end{array} \right\}, \tag{2}$$

where $\boldsymbol{M}_S$, $\boldsymbol{C}_S$ and $\boldsymbol{K}_S$ represent the structural mass, damping and stiffness matrices, respectively. The right hand side represents the aerodynamic forces and moments, where $q$ is the dynamic pressure. $\boldsymbol{A}$ is the matrix of aerodynamic

coefficients expressed as:

$$\boldsymbol{A}\left(s'\right) = 2b^2\left(\boldsymbol{M}^{NC}s'^2 + \left(\boldsymbol{C}^{NC} + \mathscr{C}\left(s'\right)\boldsymbol{r}_1\boldsymbol{s}_2^T\right)s' + \boldsymbol{K}^{NC} + \mathscr{C}\left(s'\right)\boldsymbol{r}_1\boldsymbol{s}_1^T\right), \tag{3}$$

where $\boldsymbol{M}^{NC}$, $\boldsymbol{C}^{NC}$, $\boldsymbol{K}^{NC}$ are the non-circulatory mass, damping and stiffness matrices, respectively, $b$ is the reference semi-chord length. Products $\boldsymbol{r}_1\boldsymbol{s}_2^T$ and $\boldsymbol{r}_1\boldsymbol{s}_1^T$ define the circulatory terms, where $\boldsymbol{r}_1$, $\boldsymbol{s}_1$ and $\boldsymbol{s}_2$ are $3\times 1$ column vectors of coefficients. The complex Theodorsen lift-deficiency function is noted $\mathscr{C}\left(s'\right)$, where the reduced frequency is $s' = sb/U$, $U$ being the flow speed.

To handle arbitrary motions, a time domain model is also considered in this work. This form of the model provides for a state-space representation of the system by using Duhamel's integral of Wagner indicial step response, leading to a linear time invariant (LTI) model that can be readily analyzed using LTI system theory (Leishman, 2006). The aeroelastic model writes in this case

$$\boldsymbol{M}_S\begin{Bmatrix}\ddot{h}\left(t\right)/b\\ \ddot{\theta}\left(t\right)\\ \ddot{\delta}\left(t\right)\end{Bmatrix} + \boldsymbol{C}_S\begin{Bmatrix}\dot{h}\left(t\right)/b\\ \dot{\theta}\left(t\right)\\ \dot{\delta}\left(t\right)\end{Bmatrix} + \boldsymbol{K}_S\begin{Bmatrix}h\left(t\right)/b\\ \theta\left(t\right)\\ \delta\left(t\right)\end{Bmatrix} = 2qb^2\begin{Bmatrix}-C_L^{NC} - C_L^C - C_L^G\\ C_M^{NC} + C_M^C + C_M^G\\ C_H^{NC} + C_H^C + C_H^G\end{Bmatrix}, \tag{4}$$

where $(\cdot)^{NC}$ identifies non-circulatory terms, $(\cdot)^C$ refers to the circulatory ones, while $(\cdot)^G$ indicates terms related to the turbulent flow fluctuations. The non-circulatory terms written in matrix form correspond to the non-circulatory terms in matrix $\boldsymbol{A}$ of Eq. (2). On the other hand, the circulatory terms are defined as:

$$C_L^C = C_{L_{/\alpha}}\alpha^C + C_{L_{/\delta}}\delta^C, \tag{5a}$$

$$C_M^C = \left(a + \frac{1}{2}\right)C_L^C, \tag{5b}$$

$$C_H^C = C_{H_{/\alpha}}\alpha^C + C_{H_{/\delta}}\delta^C, \tag{5c}$$

where $a$ is the non-dimensional distance between the elastic axis and the section mid chord, whereas $C_{L/*}$ and $C_{H/*}$ represent the partial derivatives of the lift and hinge moment coefficients with respect to the generic parameter $*$, i.e. the angle of attack $\alpha$ or the flap deflection $\delta$. The circulatory angles $\alpha^C$ and $\delta^C$ are computed as:

$$\alpha^C = \alpha_{QS}\left(0\right)\varphi\left(\tau\right) + \int_0^\tau \frac{\mathrm{d}\alpha_{QS}\left(\sigma\right)}{\mathrm{d}\sigma}\varphi\left(\tau-\sigma\right)\mathrm{d}\sigma, \tag{6a}$$

$$\delta^C = \delta_{QS}\left(0\right)\varphi\left(\tau\right) + \int_0^\tau \frac{\mathrm{d}\delta_{QS}\left(\sigma\right)}{\mathrm{d}\sigma}\varphi\left(\tau-\sigma\right)\mathrm{d}\sigma, \tag{6b}$$

where $\tau = tU/b$ is the traveled distance expressed in semi-chord lengths $b$. Function $\varphi(\cdot)$ is the Jones approximation of Wagner function (c.f. Leishman, 2006), while the quasi-steady $(\cdot)_{QS}$ angles are given by

$$\alpha_{QS} = U\theta + \frac{\dot{h}}{b} + b\left(\frac{1}{2} - e\right)\dot{\theta}, \tag{7a}$$

$$\delta_{QS} = \frac{U}{\pi}\left(T_{10} - lT_{21}\right)\delta + \frac{b}{2\pi}\left(T_{11} - 2lT_{10}\right)\dot{\delta}. \tag{7b}$$

Coefficients $T_{ij}$ depend on the geometrical configuration of the flap (for their expressions, see Theodorsen and Garrik, 1942), while $e$ is the distance between flap hinge and mid chord point, and $l$ the one from flap hinge to the airfoil trailing edge. The lift and pitch moment coefficients are defined as:

$$C_L^G = C_{L_{/\alpha}} \alpha^G, \tag{8a}$$

$$C_M^G = \left(a + \frac{1}{2}\right) C_L^G. \tag{8b}$$

The angle of attack $\alpha^G$ is obtained as the solution of Küssner problem for an arbitrary vertical gust profile, which gives (Leishman, 2006):

$$\alpha^G = \alpha^G(0)\,\psi(\tau) + \int_0^\tau \frac{\mathrm{d}\alpha(\sigma)}{\mathrm{d}\sigma}\psi\,(\tau-\sigma)\,\mathrm{d}\sigma, \tag{9}$$

where $\psi(\cdot)$ is the exponential approximation of Küssner function. The hinge moment coefficient generated by a vertical gust profile has the following expression:

$$C_H^G(\tau) = \frac{1}{2qb^2}\int_b e^b \Delta\bar{p}_a(x) e^{ik\tau}(x-be)\,\mathrm{d}x, \tag{10}$$

where $\Delta\bar{p}_a(x)$ is Schwarz complex solution (Bisplinghoff and Ashley, 1962). The expression for $C_H^G$ given by Eq. (10) does not lead to a state space form of the model governing equations. To correct for this, Kanda and Dowell (2005) proposed to assume the upwash caused by the gust as constant over the section, which means that the circulatory contribution caused by the sectional motion is the same as the one due to the gust, an assumption that is acceptable for reduced frequencies $s' \ll 1$. This way, $\tilde{\alpha}^G$ can be expressed as

$$\tilde{\alpha}^G = \tilde{\alpha}^G(0)\,\phi(\tau) + \int_0^\tau \frac{\mathrm{d}\alpha(\sigma)}{\mathrm{d}\sigma}\phi(\tau-\sigma)\,\mathrm{d}\sigma \approx \alpha^G, \tag{11}$$

which gives:

$$C_H^G = C_{H_{/\alpha}} \tilde{\alpha}^G. \tag{12}$$

Finally, Duhamel integrals are solved by state space realization.

The resulting system model can be expressed in LTI form as

$$\dot{\boldsymbol{x}} = \boldsymbol{A}\boldsymbol{x} + \boldsymbol{B}\boldsymbol{u}. \tag{13}$$

The state vector is noted $\boldsymbol{x}$, and contains both structural and aerodynamic states. The structural degrees of freedom include the plunge displacement, the torsional rotation and the flap deflection, together with their respective time rates. The aerodynamic states are related to the indicial response, including the approximation of the Wagner function and the one of the Küssner function for unsteady loads. The input vector $\boldsymbol{u}$ contains the turbulent fluctuations of the angle of attack and the collective-pitch control input.

## 3. Flap sizing, results and discussion

The proposed passive flap concept was applied to the DTU 10 MW reference wind turbine (RWT), which represents a significant example of the next generation very large HAWTs. The DTU 10 MW RWT is a conceptual machine developed by Danmarks Tekniske Universitet (DTU), freely availably in the public domain for research purposes (DTU RWT, 2015). The main characteristics of the wind turbine are reported in Table 1, while a more complete description of the model is given by Bak et al. (2015).

| Parameter | Value |
|---|---|
| Rotor diameter | 178.3 m |
| Hub height | 119.0 m |
| Wind class | IEC 1A |
| Rated power | 10 MW |
| Cut-in wind speed | 4 m/s |
| Cut-out wind speed | 25 m/s |

Table 1: Main parameters of the DTU 10 MW RWT.

In the following, the flap is sized and its main performance characteristics are evaluated by means of numerical simulations. At first, we consider the problem of aerodynamic balancing, which leads to a choice for the hinge location. Next, the flap is optimized in order to yield the best possible alleviation of fatigue damage, while ensuring a stable response throughout the entire operating envelope of the machine. A transfer function analysis is then used to illustrate the notch filtering action realized by the flap on angle of attack fluctuations in the frequency band that is most responsible for the generation of fatigue damage. The study is concluded by verifying that passive flaps do not affect in a noticeable manner the power production of the machine, nor increase the ultimate loads encountered in emergency shutdown conditions.

### *3.1. Aerodynamic balancing and mitigation of speed dependency*

Aerodynamic balancing refers to the reduction of the effects of changes in angle of attack on hinge moments, which are captured by the $C^C_{H_{/\alpha}}$ derivative. A small (ideally null) value of this derivative helps reducing the interaction between the passive device and the active pitch control system of the wind turbine. Indeed, the passive flap should not contrast the activity of the pitch controller, but should only react to changes in angle of attack due to blade vibrations. An aerodynamically balanced flap effectively decouples the flap motion and blade pitch, achieving the desired independence of the passive and deliberate active responses.

Aerodynamic derivatives are estimated here by thin airfoil theory, as described in Theodorsen and Garrik (1942), which allows for the evaluation of the aerodynamic coefficients by analytical expressions. In reality, the aerodynamic

derivatives of the flap are also influenced by the local shape and gap between airfoil and flap, as well by fluid viscosity. For these reasons, the results provided by thin airfoil theory can be considered only as approximate estimates, which are nonetheless sufficient for the scopes of the present study.

A balanced flap can be typically obtained by displacing the hinge location aft of the flap leading edge. To find the balancing condition, consider the quasi-steady flap terms in Eq. (3), which read $C^C_{H_{/\alpha}} = \frac{1}{2} r_{13} s_{12}$. Balancing may be obtained by setting $r_{13} = 0$, which corresponds to an appropriate choice of the overhang, defined as the surplus part of the flap ahead of the hinge divided by the flap chord.

Sizing of the device should also consider that the effective aeroelastic stiffness of the flap depends on flow speed. This is in general an undesirable effect because it tends to detune the flap, thereby reducing its efficacy in certain operating ranges, and it may possibly also affect its stability. In fact, from Eq. (2), the aeroelastic flap stiffness $k^{AS}_{\delta}$ can be written as

$$k^{AS}_{\delta} = k_{\delta} - \frac{1}{2}\rho U^2 c^2 \left( C^{NC}_{H_{/\delta}} + \mathscr{C}\left(s'\right) C^{C}_{H_{/\delta}} \right), \tag{14}$$

where $\rho$ is the air density. This expression shows how the aeroelastic stiffness depends on flow speed through terms $C^{NC}_{H_{/\delta}} = \frac{1}{2} K^{NC}_{33}$ and $C^{C}_{H_{/\delta}} = \frac{1}{2} r_{13} s_{13}$. While the latter term is null for a balanced flap, i.e. when the balancing condition $r_{13} = 0$ is satisfied, the former could also be rendered equal to zero by an appropriate sizing. A better approach, however, is to use it for compensating the centrifugal stiffening term in $k_{\delta}$ (cf. Eq. (1)), which, depending on rotor speed, is also related to sectional speed.

Figure 3 shows the non-circulatory term $C^{NC}_{H_{/\delta}}$ as a function of the overhang, for a flap chord equal to 10% of the sectional chord. By examining the plot, it appears that an overhang equal to 32% makes the non-circulatory term equal to zero, while larger values (corresponding to positive values of this aerodynamic derivative) can be chosen to compensate the (negative) centrifugal stiffening effects.

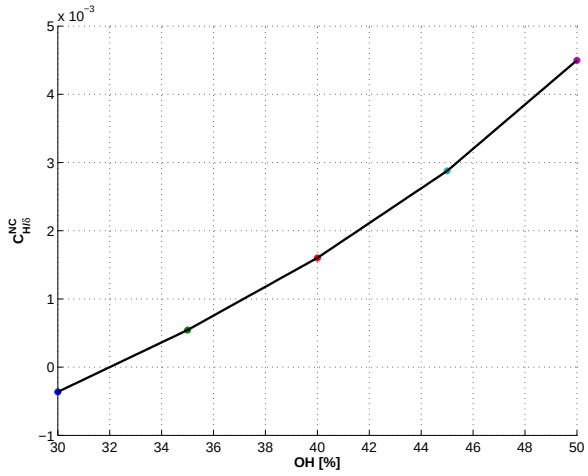


Figure 3: Non-circulatory component of hinge moment derivative $C^{NC}_{H_{/\delta}}$ as a function of overhang OH, expressed as a percentage of flap chord.

In order to verify the effect of balancing in its ability not to affect changes in angle of attack due to pitching, the plunge and torsional degrees of freedom of the 2D typical section model were frozen, while the flapped airfoil was subjected to turbulent wind fluctuations. Figure 4 shows the time histories of lift (at top) and flap deflections (at bottom) for two mean wind speeds. The lift plots for the cases with and without flap are nearly identical, indicating that the flap generates negligible aerodynamic forces. Similarly, the bottom plots show that the flap deflection is very small, as hinge moments are nearly insensitive to changes in angle of attack. These results confirm that, when the blade is not vibrating, the flap essentially does not move even if the flow is fluctuating. On the other hand, when the blade vibrates, accelerations transmitted to the balancing mass are responsible for making the flap respond.

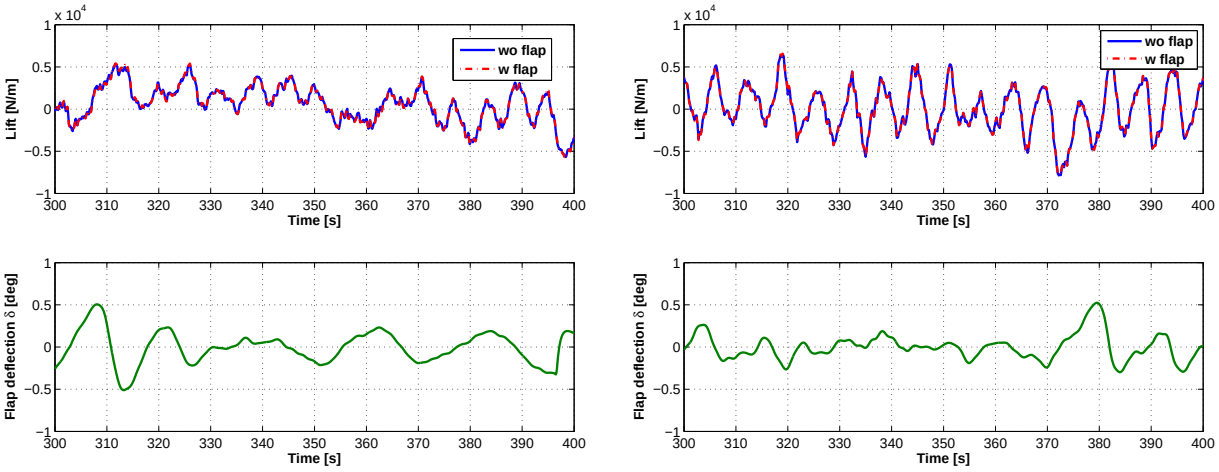


(a) Hub wind speed of 13 m/s.

(b) Hub wind speed of 25 m/s.

Figure 4: Lift (top) and flap deflection (bottom) vs. time at different mean wind speeds, while freezing the plunge and twist degrees of freedom.

### *3.2. DEL-based sizing*

The span-wise position of the passive flap is placed in this study at 75% of blade length. Although this could be further optimized, this location offers a reasonable compromise in terms of effectiveness on the control of the first blade modal shape, while still offering a not too small chord length and sectional thickness. In fact, the thickness of the section limits the possible excursion of the balancing mass, thereby limiting the flap motion and authority. Some relevant blade and sectional parameters are reported in Table 2 (Bak et al., 2012).

As the main goal of the passive flap is the reduction of fatigue loading, fatigue was used as the principal metric driving the sizing of the device. Fatigue is here measured in terms of lifetime damage equivalent loads (DEL). The DEL of the plunge displacement of the typical section is considered as an indicator of the flapping motion of the entire blade, and hence of the associated root bending moment. According to this model, a reduction of the plunge DEL of the typical section is interpreted as an increase in the fatigue life of the blade.

| Parameter | Value |
|---|---|
| Chord | 3.25 m |
| Plunge frequency | 0.62 Hz |
| Torsional frequency | 4.99 Hz |
| Plunge damping factor | 0.01 |
| Torsional damping factor | 0.01 |
| Sectional mass | 186 Kg/m |
| Sectional moment of inertia | 94.1 Kgm |
| Elastic axis position from leading edge | 35% blade chord |
| Static moment | 6.25% blade chord |

Table 2: Blade and sectional parameters for the DTU 10 MW RTW. Sectional data correspond to 75% span.

DELs are estimated on the 2D typical section model, under flow conditions computed on the 3D closed-loop aeroservoelastic model. The 2D model therefore feels the effects of flow fluctuations due to vertical wind shear, turbulence and pitch activity. Notice that this is a conservative estimation of DEL, as in a tightly coupled simulation (and in reality) the typical section would feel reduced flow fluctuations resulting from its reduced oscillations. Simulations are conducted at different wind speeds in order to cover the entire operating range of the machine, and for multiple realizations of the turbulent wind field, as prescribed by certification guidelines (IEC 61400-1, 2005; GL, 2010). Lifetime DELs are then obtained by weighting with a Weibull probability function (Hansen, 2008).

To identify the best passive flap configuration, DELs are computed for varying values of the flap frequency, damping and chord length. The fraction of sectional chord occupied by the flap clearly plays an important role. In fact, reducing the chord occupation reduces the effectiveness of the flap. At the same time, its maximum allowable excursion is also limited, as the airfoil is thinner towards its trailing edge. On the other hand, too large a flap should be avoided as the balancing mass would start interfering with the aft shear web of the blade. Analyzing the various requirements and the results of simulations, a good compromise was found for a flap chord equal to 16% of the sectional chord, with a distance of the offset mass from the hinge axis equal to 32% of the sectional chord.

Figure 5 reports the iso-contours of the DEL percent reduction with respect to the baseline unflapped blade, computed as previously explained, as a function of flap frequency and damping. Looking at the plot, it appears that low flap modal frequencies are associated with larger DEL reductions. The reason for this behavior will become clear in the response function analysis conducted later on. However, stability limits the flap frequency from below, as shown by the shaded area in the graph that indicates unstable combinations of parameters. A reasonable choice appears to be a modal frequency equal to 0.032 Hz, which corresponds to a DEL reduction of 35%. The figure shows that iso-contour lines in that region of the plot are essentially unaffected by the damping factor. At the light of this consideration, the

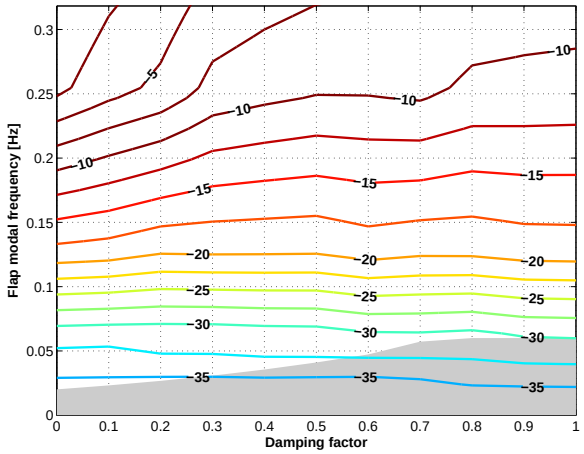


Figure 5: Lifetime DEL percent reduction with respect to the baseline unflapped blade, as a function of flap frequency and damping. The shaded area represents unstable configurations.

flap is realized without a hinge damper, which also helps keep the solution away from the stability limit. A value of the damping factor equal to 0.1 was used in the numerical simulations, to account for the possible presence of friction in the rotation mechanism; however, the plot shows that results are very robust to this possibly uncertain parameter. Values of the flap parameters corresponding to these choices are reported in Table 3.

| Parameter | Value |
|---|---|
| Chord | 0.51 m |
| Modal frequency | 0.032 Hz |
| Damping factor | 0 |
| Mass | 5.6 Kg/m |
| Static moment | 16% blade chord |
| Moment of inertia | 4.19 Kgm |
| Overhang | 31.9% flap chord |
| Flap free-play range | -22.5 deg $< \delta <$ 15.1 deg |

Table 3: DEL-optimized parameters of the passive flap.

### *3.3. Stability analysis*

The stability of the system is verified next.

Figure 6(a) shows the V-g (Hodges and Pierce, 2002), or speed-damping, diagram for a range of hub-height wind speeds from cut-in to cut-out. The solutions corresponding to the passive flap case are reported using solid lines, while

the ones without flap by dash-dotted lines. Using the V-g method, a structural damping term $g$ is added in order to bring each mode to the verge of flutter, i.e. to a purely periodic response. For each considered speed, if the resulting $g$ is smaller than the actual structural damping, than the system is stable. The plot shows that the flapped typical section if flutter-free in its entire range of operating conditions, as $g$ is always largely negative.

It appears that the addition of the flap has very limited effects on the torsional mode. On the other hand, the damping of the plunge mode is somewhat affected, but without creating any stability problem. The flap mode is also well damped throughout the entire operating range. This is largely due to the mitigation of speed dependency of the aerodynamic derivatives of the model achieved through aerodynamic balancing and flap sizing, as explained earlier on.

Figure 6(b) shows the system modal frequencies as functions of rotor speed, the plot showing the typical effects of centrifugal stiffening. Here again frequencies are well separated and coalescence of the plunging and torsional modes is far outside of the operating conditions. The frequency of the flap mode is essentially constant, and this is again due to aerodynamic balancing and its effects on the mitigation of the dependency of the model coefficients on flow speed.

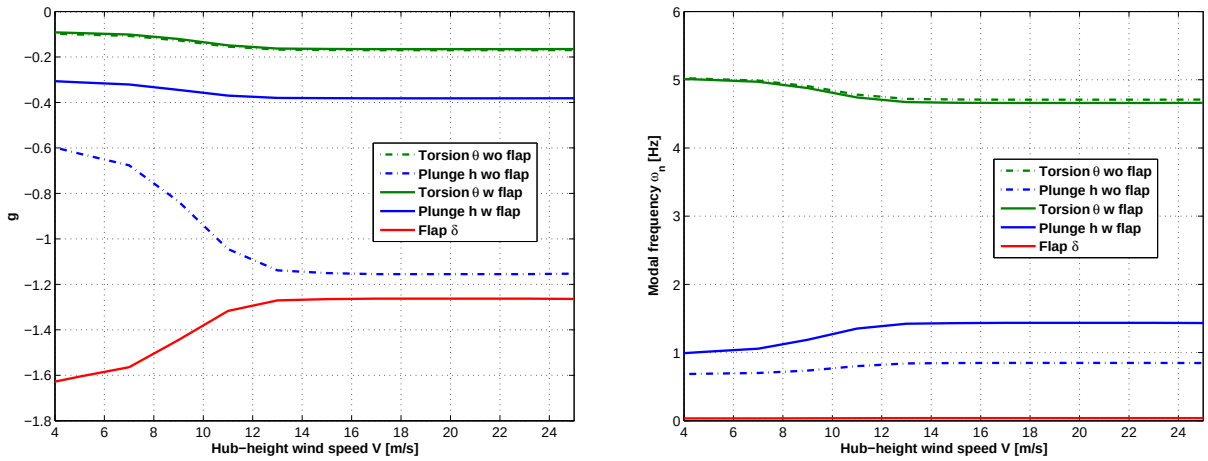


(a) V-g plot.

(b) Modal frequencies vs. wind speed speed.

Figure 6: Stability and frequency analysis of the flapped typical section.

### *3.4. Transfer functions analysis*

To better understand the effects of the passive flap on the response of the system, the transfer functions of the three degrees of freedom of the flapped typical section are computed next, using the state space model.

Figure 7 shows the transfer functions from angle of attack to plunge, torsion and flap deflection. The transfer functions of the system with passive flap are reported by solid lines, while the case without flap is represented by dash-dotted lines. The plot corresponds to operation at rated wind speed.

Examining the plunge transfer function, there is a strong reduction in magnitude around the band 1P-3P when the passive device is used. This transfer function presents two peaks: a mild one in correspondence of the frequency of

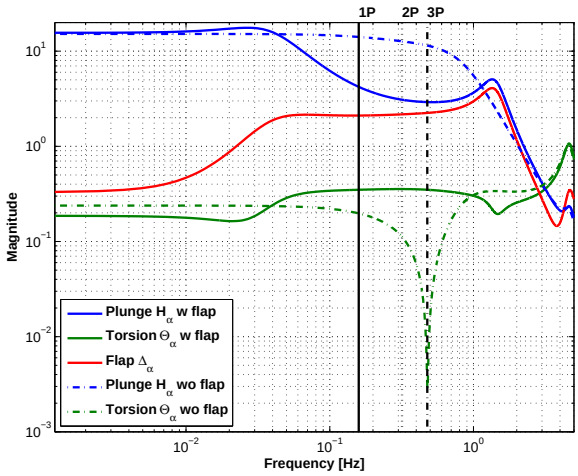


Figure 7: Transfer functions between angle of attack and plunge, torsion and flap deflection for operation at rated wind speed.

the flap around 0.032 Hz, and one at the new plunge frequency around 1.5 Hz, which is slightly higher than in the case without flap, as already shown by Fig. 6(b).

The flap transfer function is essentially null below the flap natural frequency. This is obtained by design, and it is due to the use of aerodynamic balancing. On the other hand, the flap responds at higher frequencies up to the plunge one, after which its contribution quickly dies off. These results show that the passive flap effectively behaves as a notch filter in the 1P-3P band. The synergy between plunge and flap is due to the fact that the two frequencies are quite close to each other. On the other hand, the torsional motion remains largely unaffected by the presence of the flap.

Figure 8 shows the transfer function from angle of attack to plunge for varying wind speed. The plot at left corresponds to the case without flap, while the one at right is for the passive flap case. Here again it appears that the passive flap is capable of creating a very noticeable attenuation in the 1P-3P band, which remains remarkably constant throughout the entire range of operating wind speeds of interest.

The attenuation exhibited by the passive flap in the 1P-3P band is crucial for the reduction of fatigue loading on the wind turbine. In fact, fatigue is primarily generated in this range of frequencies, and not much of it is caused by fluctuations above the 3P. This is shown by Fig. 9, which reports the normalized blade root lifetime DEL bending moment as a function of load harmonics, as computed for the baseline RWT by using the 3D aeroservoleastic model. It appears that DEL increases very rapidly with frequency, to the point that already 75% of damage is accumulated for frequencies up to 1P, and then levels off, with very little contributions coming from frequencies above the 3P.

### *3.5. Turbulent wind simulations and fatigue*

The effectiveness of the passive flap concept is then evaluated by means of time domain simulations in turbulent wind conditions. The 3D aeroservoelastic model provides the angle of attack time histories that are used for feeding the 2D typical section model, realizing a one-way coupling between the two models. Figures 10 through 12 report results

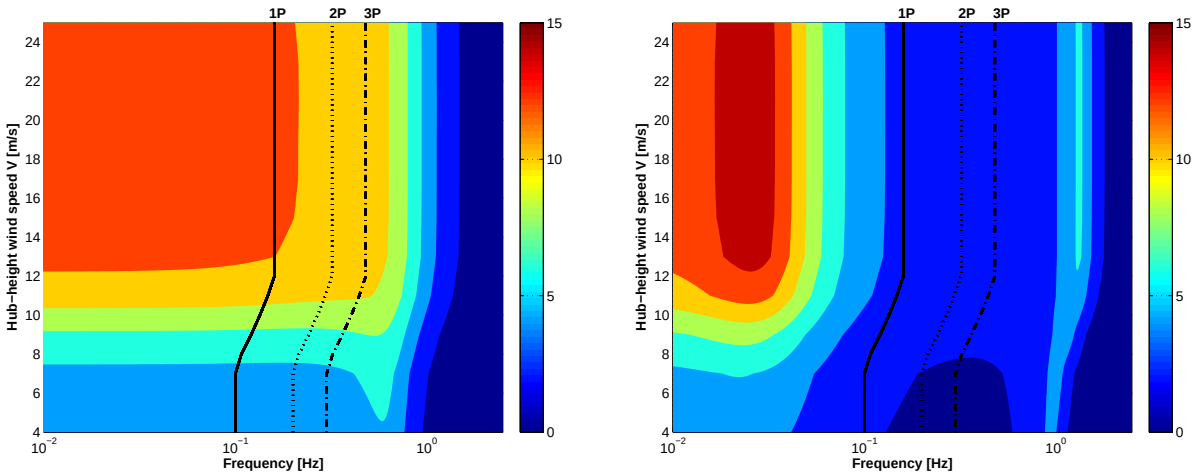


(a) Unflapped baseline configuration.

(b) Section with passive flap.

Figure 8: Transfer functions from angle of attack to plunge motion, as functions of hub-height wind speed.

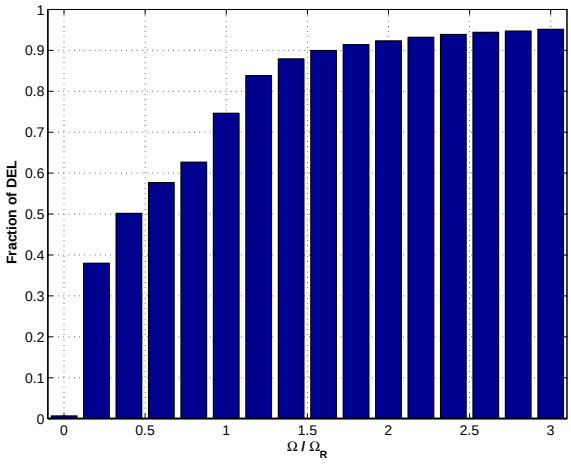


Figure 9: Normalized blade root lifetime DEL bending moment, plotted as a function of load frequency.

obtained for wind speeds of 5 m/s (close to cut-in), 13 m/s (rated) and 25 m/s (cut-out).

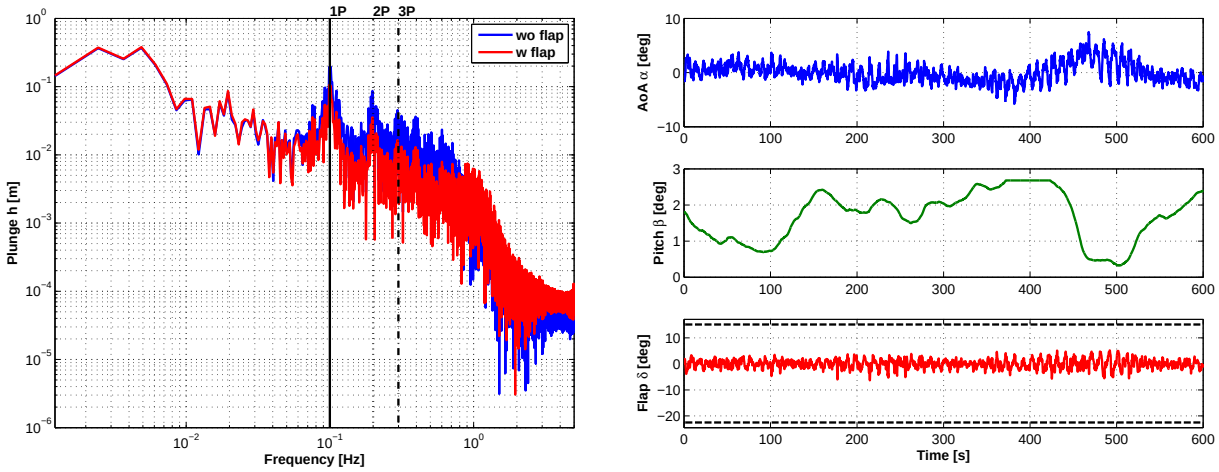


(a) Plunge response spectrum.

(b) Time histories of inputs and flap response.

Figure 10: System response around 5 m/s (cut-in).

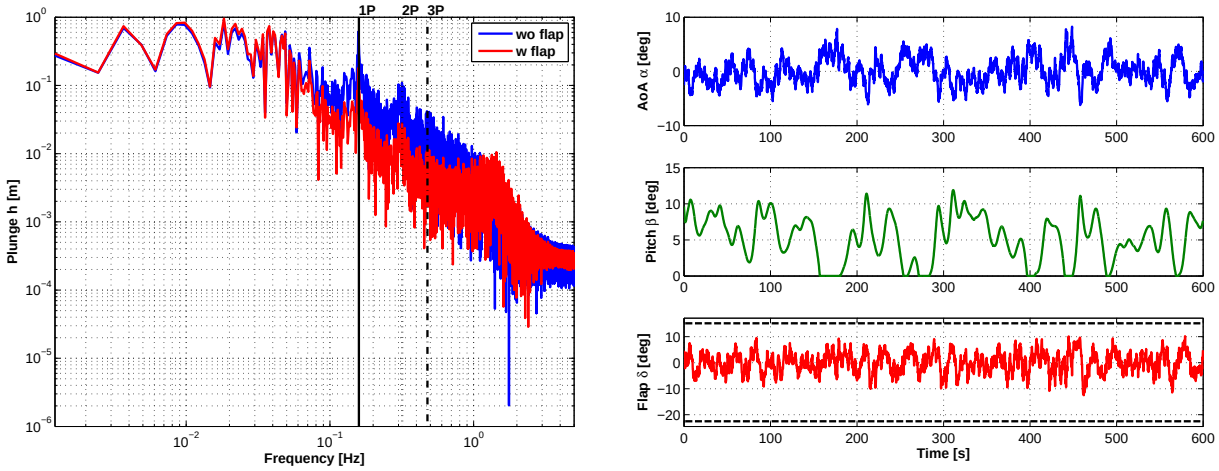


(a) Plunge response spectrum.

(b) Time histories of inputs and flap response.

Figure 11: System response around 13 m/s (rated).

Figures 10(a), 11(a) and 12(a) report the spectrum of the plunge response with and without passive flap. The peaks at the 1, 2 and 3P are very noticeable, as expected. In all cases, peaks are very significantly reduced by the passive flap in the 1P-3P band.

Figures 10(b), 11(b) and 12(b) report, from top to bottom, the time histories of the angle of attack, pitch angle and flap deflection. The pitch activity differs significantly in the various plots, on account of the difference in control strategy that is used for regulating the machine throughout different ranges of wind speeds. The flap deflection plots report

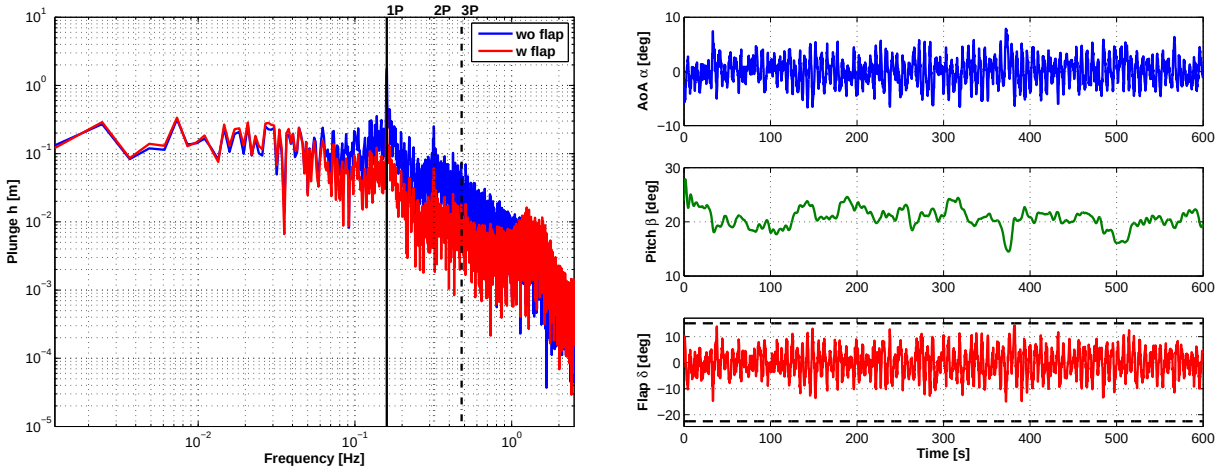


(a) Plunge response spectrum.

(b) Time histories of inputs and flap response.

Figure 12: System response around 25 m/s (cut-out).

with black dashed lines the limits of allowable flap deflections, which are constrained by the fact that the balancing mass is restricted to move within the pressure and suction sides of the airfoil. It appears that the maximum allowable excursions are achieved only very seldom and exclusively for the highest wind speed conditions, confirming the correct sizing of the device even from this point of view.

Fatigue damage, as captured by DELs of the typical section plunging motion, is shown in Fig. 13 for varying wind speeds. The results for the configuration without flap are reported by blue bars, while red bars are used for the rotor equipped with the passive flap. Figure 13(a) reports DELs accumulated at each single wind speed. It appears that DELs are particularly high around rated and cut-out, wind speed ranges where the largest loads typically occur. This figure shows in particular how the flap is effective at all wind speeds. A different view is offered by Fig. 13(b), which reports DELs weighted by the Weibull wind probability. The figure shows that the most significant contributions to DELs come from the wind speed range around rated. Summing up over the complete wind range gives the lifetime DEL, which was previously shown in Fig. 5. All plots confirm the very significant attenuation of DELs given by the use of the passive flap.

### *3.6. Effects on power production*

The effects on power production are estimated by the closed-loop loosely-coupled hybrid model described earlier on. The aerodynamic force perturbations generated by the 2D sectional model at each time instant are applied back onto the 3D aeroservoelastic model. Simulations are conducted in NTM wind conditions for different values of mean wind speed covering the entire wind speed range. Results are shown in Fig. 14, which reports the mean value of the electrical power vs. mean hub-height wind speed. The plot shows a very limited effect of the use of the passive flap on power production.

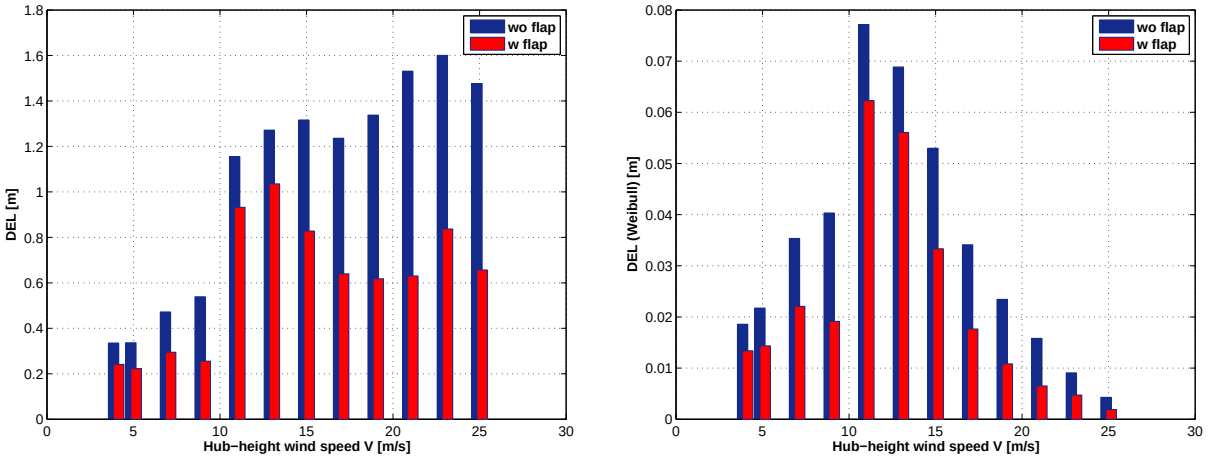


(a) Blade DELs vs. wind speed.

(b) Weibull-weighted blade DELs vs. wind speed.

Figure 13: DELs of the typical section plunging motion, with and without passive flap.

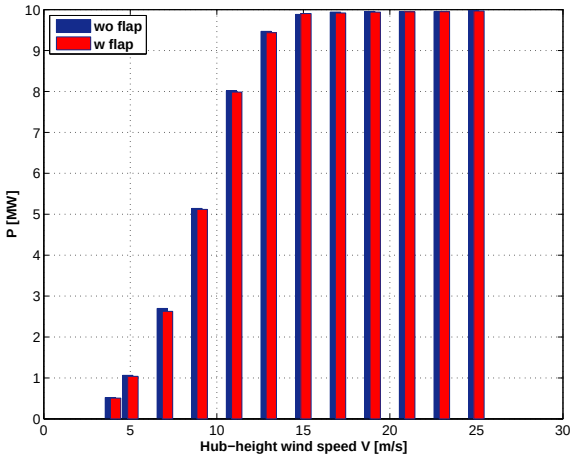


Figure 14: Power production in turbulent condition for varying mean wind, with and without passive flap.

Weighting the results of Fig. 14 with the Weibull distribution, yields the annual energy production (AEP). The use of the flap incurs in a reduction in AEP of 0.33% with respect to the badeline unflapped case, which is a modest and acceptable amount.

### *3.7. Ultimate load analysis*

Ultimate loads are often generated during emergency shutdowns when, during a strong gust and concomitant loss of connection to the grid, the machine enters into a rapid aerodynamic braking of the rotor by pitching the blades to feather (cf. DLC 2.3 IEC 61400-1, 2005). This violent maneuver not only rapidly slows down the rotor, but also makes the machine spring forward, due to the sudden drop and reversal of thrust. Given the fact that the loads generated during these maneuvers are often design drivers, it is important to verify that the use of the passive flap does not increase such ultimate loads.

Figure 15 shows the results for an emergency shutdown conducted following a deterministic gust at cut-out, with grid loss at the point of maximum gust peak.

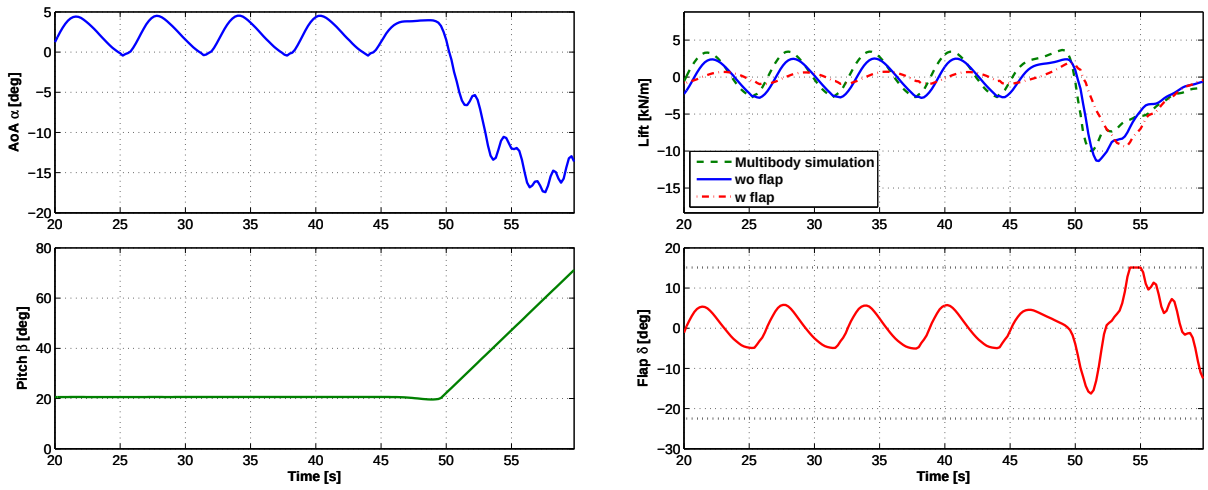


(a) Angle of attack and pitch time histories.

(b) Lift and flap deflection time histories.

Figure 15: Emergency shutdown following an extreme operating gust with concomitant grid loss at cut-out wind speed.

Figure 15(a) reports the time histories of the angle of attack at the blade section (top) and the blade pitch (bottom). The second plot clearly shows the rapid pitch to feather of the blade commanded by the control system in order to rapidly slow down the rotor.

The top part of Fig. 15(b) compares the lift time history for the 3D multibody simulation of the baseline unflapped rotor (green dashed line), the 2D sectional model without flap (blue solid line), and the 2D sectional model with flap (red dash-dotted line). There is a good matching between the multibody model and the sectional model without flap, which supports the validity of the loose coupling strategy. The load peak, which is achieved during the first swing

forward oscillation of the machine, is a little more pronounced and slightly delayed for the sectional model. On the other hand, the response of the flapped section is much smoother because of the load mitigating action of the device, which drastically reduces the prominent 1P oscillation visible in the unflapped case. The load peak is also smaller and delayed. The bottom part of the figure plots the time history of the flap deflection, showing that the flap hits the limits of its allowed free deflection during the maneuver. Suitable end stops will have to be designed, in order to cope with the reaching of limit flap excursions in these extreme conditions.

For all possible combinations of gust and grid loss time (IEC 61400-1, 2005), Fig. 16 shows the plunge peak for the unflapped and flapped cases. Here again, as in the case of the fatigue analysis, plunge motion is assumed to be well correlated with loads, and it is therefore used as the relevant metric for this analysis. Looking at the results, it appears that even in this case, although this is not its primary goal, the passive device realizes some reductions in the loads.

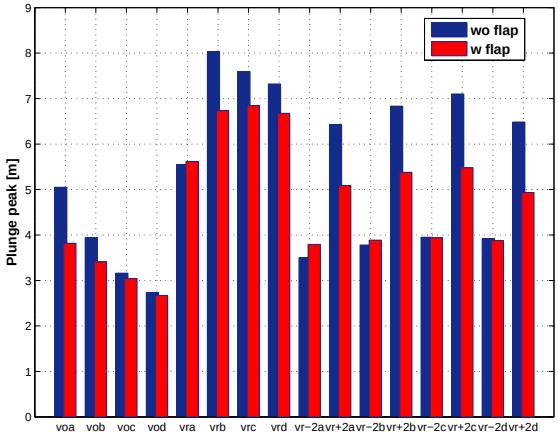


Figure 16: Ultimate (plunge) peaks for extreme operating gust with concomitant electrical loss, DLC 2.3, for the flapped and unflapped cases.

## 4. Conclusions

In this paper a new passive device concept for load mitigation has been proposed. The idea, as implemented by means of a freely moving flap, has been preliminarily investigated with regard to a conceptual 10 MW machine. The advantage of this solution is that it does not require sensors nor actuators because it moves passively in response to blade vibrations, an advantage that might be particularly beneficial for offshore applications.

Ad-hoc simulation models were developed to conduct the present study. The models include a typical section of the blade with unsteady aerodynamics described by thin airfoil theory in the frequency and time domains. This model was used for sizing the main parameters of the passive flap and to evaluate the system response to angle of attack inputs. A tuning procedure of the flap parameters was presented, that maximizes DEL mitigation while ensuring stability. The typical section was coupled to a closed-loop aeroservoelastic model of the wind turbine. This second model was used for providing angle of attack driving inputs to the typical section, and to estimate power production by correcting

a posteriori the blade aerodynamic forces based on the typical section results. Various analyses were conducted to evaluate relevant performance metrics with and without the passive flap.

The results obtained so far seem to indicate that the proposed concept has some interesting potential:

- The optimal flap parameters are very reasonable, and do not require excessive size nor masses.
- Fatigue load alleviation is very noticeable, and accompanied only by modest AEP reductions
- The behavior is robust and consistent within the entire operating regime of the wind turbine, without necessitating of scheduling of system parameters with respect to wind speed or other quantities. To this end, an instrumental role was played by a sizing of the flap that performs an approximate cancellation of the effects due to centrifugal forces and non-circulatory aerodynamics.
- The solution is compatible with standard active blade pitch control strategies, routinely adopted on board modern wind turbines. In fact, differently from other passive flap concepts, the present device does not respond to deliberate changes in angle of attack due to active blade pitching.
- The flap concept appears to be applicable without the need for radical changes in the design of blades (although, to fully exploit the benefits of the passive device, it is expected that a passive-flap-equipped blade will have to be redesigned, for example by increasing its span, reducing its weight, or resizing some of its components).
- There is the potential also for the reduction of ultimate stresses during violent transients, as in emergency shut-down procedures.

The continuation of this study will make use of more sophisticated simulation models, whereby the passive flap will be implemented within a complete aeroservoelastic model of the machine, improving on the current loosely-coupled approach. The integration of the passive flap concept with other active (e.g. individual blade pitch) and/or passive (e.g. BTC) technologies will be investigated in the more general framework of rotor design. In addition, the alternative embodiment of the new concept proposed here in a freely pitching tip will be studied.

**Acknowledgements**

Support of the FP7 INNWIND.EU project to the Politecnico di Milano is gratefully acknowledged.

**References**

DTU 10 MW Reference Wind Turbine Project. Web site: http://dtu-10mw-rwt.vindenergi.dtu.dk.

Guideline for the Certification of Wind Turbines, Ed. 2010. Germanischer Lloyd Industrial Services GmbH, Renewables Certification, Brooktorkai 10, 20457 Hamburg, Germany.

Wind Turbines — Part 1: Design Requirements, Ed. 3. International Standard IEC 61400-1, 2005.

Arrieta, A.F., Bilgen, O., Friswell, M.I., Hagedom, P., 2012. Passive load alleviation bi-stable morphing concept. AIP Advances, 2, DOI: 10.1063/1.4739412.

Arrieta, A.F., Kuder, I.K., Rist, M., Waeber, T., Ermanni, P., 2014. Passive load alleviation aerofoil concept with variable stiffness multi-stable composites. Composite Structures, 116, 235–242, DOI:10.1016/j.compstruct.2014.05.016.

Bak, C., Bitsche, R., Yde, A., Zahle, F., Gaunaa, M., Blasques, J., Døssing, M., Heinen, J.J.W., Behrens, T., 2012. DTU 10 MW Reference Wind Turbine Project. http://orbit.dtu.dk/fedora/objects/orbit:111503/datastreams/file_7946742/content.

Bak, C., Zahle, F., Bitsche, R., Kim, T., Yde, A., Henriksen, L.C., Andersen, P.B., Natarajan, A., Hansen, M.H., 2015. Design and performance of a 10 MW wind turbine. Wind Energy, to appear.

Bauchau, O.A., Bottasso, C.L., Trainelli, L., 2003. Robust integration schemes for flexible multibody systems. Computer Methods in Applied Mechanics and Engineering, 192, 395–420, DOI:10.1016/S0045-7825(02)00519-4.

Bauchau, O.A., Epple, A., Bottasso, C.L., 2009. Scaling of constraints and augmented Lagrangian formulations in multibody dynamics simulations. Journal of Computational and Nonlinear Dynamics, 4(2), DOI:10.1115/1.3079826.

Bielawa, R.L, 1984. Analytic Investigation of Helicopter Appended Aeroelastic Devices. NACA Report 166525, NASA Ames Research Center.

Bisplinghoff, R.L., Ashley H., 1962. Principles of Aeroelasticity. John Wiley & Sons, Inc., Hoboken, New Jersey.

Bottasso, C.L., Croce, A., 2006–2015. `Cp-Lambda` User's Manual. Dipartimento di Scienze e Tecnologie Aerospaziali, Politecnico di Milano, Milano, Italy.

Bottasso, C.L., Croce, A., Devecchi, D., Riboldi, C.E.D, Nam, Y., 2013. Multi-layer control architecture for the reduction of deterministic and non-deterministic loads on wind turbines. Renewable Energy 51, 159–169.

Doney, P., Shufflebarger, C.C., 1940. Test of a Gust-Alleviating Flap in the Gust Tunnel. Tech. Report 745, NACA.

Hansen, M.O.L., 2008. Aerodynamics of Wind Turbines, 2nd Edition. Earthscan.

Hodges, D.H., Pierce, G.A., 2002. Introduction to Structural Dynamics and Aeroelasticity. Cambridge Aerospace Series, Cambridge University Press.

Kanda, A., Dowell, H., 2005. Worst-case gust-response analysis for typical airfoil section with control surface. Journal of Aircraft, 42 (4), 956–962.

Kelley, N., Jonkman, B., 2015. NWTC Computer-Aided Engineering Tools: TurbSim. http://wind.nrel.gov/designcodes/preprocessors/turbsim/.

Lambie, B., Jain, P., Tropea, C., 2011. Passive camber change for wind turbine load alleviation. AIAA Aerospace Sciences Meeting including the New Horizons Forum and Aerospace Exposition, Orlando, Florida.

Leishman, J.G., 2006. Principles of Helicopter Aerodynamics, 2nd Edition. Cambridge University Press, Cambridge, England.

Stroub, R.H., 1982. An Analytical Investigation of the Free-Tip Rotor for Helicopters. NASA Technical Memorandum 81345.

Theodorsen, T., Garrik, I.E., 1935. General Theory of Aerodynamic Instability and the Mechanism of Flutter. Tech. Report 496, NACA.

Theodorsen, T., Garrik, I.E., 1942. Nonstationary Flow About a Wing-Aileron-Tab Combination Including Aerodynamic Balance. Tech. Report 736, NACA.

Young, L.A., 1986. The Evaluation of a Number of Prototypes for the Free-Tip Rotor Constant-Moment Controller. NASA Technical Memorandum 86664.